ACS Catalysis

Research Article

pubs.acs.org/acscatalysis

Surface ReO_x Sites on Al_2O_3 and Their Molecular Structure–Reactivity Relationships for Olefin Metathesis

Soe Lwin,[†] Christopher Keturakis,[†] Jarosław Handzlik,[‡] Philippe Sautet,[§] Yuanyuan Li,[∥] Anatoly I. Frenkel,[∥] and Israel E. Wachs*[,†]

[†]*Operando* Molecular Spectroscopy and Catalysis Laboratory, Department of Chemical Engineering, Lehigh University, Bethlehem, Pennsylvania 18015, United States

[‡]Faculty of Chemical Engineering and Technology, Cracow University of Technology, Warszawska 24, 31-155 Kraków, Poland

[§]Université de Lyon and CNRS, Institut de Chimie de Lyon, Laboratoire de Chimie, École Normale Supérieure de Lyon, 69364 Lyon Cedex 07, France

[∥]Department of Physics, Yeshiva University, New York, New York 10016, United States

Supporting Information

ABSTRACT: Supported ReO_x/Al_2O_3 catalysts were investigated for propylene metathesis as a function of surface rhenia loading and extensively characterized with in situ UV–vis, Raman, IR, XANES/EXAFS, and isotopic $^{18}O-^{16}O$ exchange studies. The experimental studies were complemented with DFT calculations using realistic models of the alumina surface. The surface ReO_x sites were found to be isolated surface dioxo $(O{=})_2ReO_2$ species, which represent the most stable surface rhenia structures on alumina as shown by DFT. Two distinct surface ReO_4 species, however, were found to be present and only slightly differ in their bridging Re–O–Al bond lengths brought about by anchoring at different sites of the Al_2O_3 support. The deformed surface ReO_4–I species preferentially anchor at more basic μ_1 Al_{IV} and μ_1 Al_{VI} sites and are difficult to activate for propylene metathesis. The surface ReO_4–II species are formed at more acidic μ_2 Al_{VI} and μ_3 Al_{VI} sites and are the catalytic active sites for propylene metathesis. The surface ReO_4–II sites were readily activated by propylene while the deformed surface ReO_4–I sites were almost not affected by propylene, with only a few sites being activated. The steady-state propylene metathesis reaction rates are much higher for the surface ReO_4–II sites than the deformed surface ReO_4–I sites. The formation of the less reactive deformed surface ReO_4–I species could be blocked by occupation of the μ_1 Al_{IV} sites with sacrificial surface TaO_x species that resulted in catalysts exclusively containing the more active surface ReO_4–II sites on alumina. This is *the first study* to demonstrate that the surface ReO_4–II sites are the precursors for the catalytic active sites for propylene metathesis by supported ReO_4/Al_2O_3 catalysts and to molecularly design olefin metathesis catalysts that exclusively contain isolated surface ReO_4–II sites.

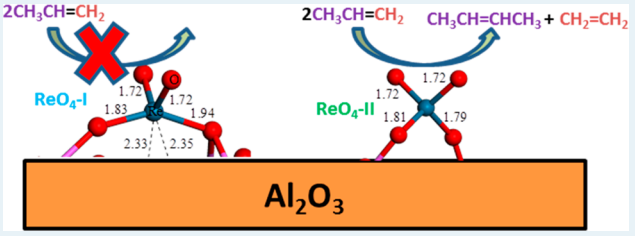

KEYWORDS: *catalysts, rhenia, alumina, olefin metathesis, spectroscopy, DFT*

1. INTRODUCTION

Supported rhenium oxide catalysts find wide applications in numerous chemical processes.[1−3] For olefin metathesis, rhenium oxide supported on Al_2O_3 stands out because it is active and selective at low temperatures.[1] The industrial importance of olefin metathesis reactions, especially to meet the current global shortage of propylene by on purpose propylene production,[4] has stimulated numerous fundamental studies about the nature of the Re^{7+} oxide catalyst precursor supported on alumina. In particular, multiple in situ characterization studies (Raman, IR, and XAS) and DFT calculations have confirmed that the surface rhenium oxide species are present as isolated sites on alumina.[5−13] The most commonly assigned molecular structure for the dehydrated Re^{7+} oxide on Al_2O_3 has been the trioxo $(O{=})_3Re-O-Al$ site (C_{3v} symmetry).[5−12] The nature of the surface Re^{7+} oxide species on alumina has recently come into question because of reported contradictory conclusions.[12,13] Bare et al. concluded that isolated trioxo $(O{=})_3Re-O-Al$ species are present for calcined supported rhenia/alumina catalysts[12] mainly from EXAFS analysis. In contrast, Scott et al. postulated isolated penta-coordinated dioxo $(O{=})_2Re(-O-Al)_3$ from XANES/EXAFS measurements and DFT calculations employing cluster models.[13] The precise coordination of the isolated surface Re^{7+} oxide species on alumina is of great importance to understand the remarkable low-temperature olefin metathesis activity of this catalyst system. Indeed, it was shown for alumina supported Mo-oxo-carbene reactive intermediate complexes that the strain induced by multiple interactions with the support can strongly enhance the catalytic properties.[14] The

Received: October 25, 2014
Revised: December 25, 2014
Published: January 21, 2015

DOI: 10.1021/cs5016518
ACS Catal. 2015, 5, 1432−1444

structural analysis of surface Re^{7+} oxide species on alumina is further complicated because two slightly different dehydrated surface rhenia species have been observed by in situ Raman spectroscopy as a function of rhenia loading.[5,6] It is, thus, of paramount importance to settle the previously mentioned Re^{7+} oxide structural debate and understand the catalytic structure−reactivity relationships for the supported ReO_x/Al_2O_3 catalyst system for olefin metathesis as a function of rhenia loading and anchoring sites on the alumina support.

In the present study, comprehensive in situ Raman, IR, UV−vis, and XANES/EXAFS experimental studies and DFT calculations are undertaken to determine the nature of surface ReO_x species on the Al_2O_3 support and their structure−reactivity relationships for olefin metathesis. The domain size or nuclearity of the surface ReO_x species are examined with in situ UV−vis spectroscopy. The average coordination of the surface ReO_x species is accessed with in situ XANES and the radial distribution of the atoms surrounding Re with in situ EXAFS. The molecular structure(s) and anchoring site(s) of the surface ReO_x species on alumina are probed with in situ Raman and IR spectroscopy, respectively, and isotopic $^{18}O/^{16}O$ exchange Raman measurements. A number of possible DFT surface models are compared for multiple surface Re^{7+}oxide sites (trioxo, dioxo, and mono-oxo coordinated rhenium oxide centers) on the (100) and (110) surfaces of γ-alumina. The alumina surfaces are described by a periodic slab.[15,16] The experimental in situ isotopic $^{18}O/^{16}O$ Raman band splitting patterns for supported ReO_x on alumina are compared with those obtained from theoretical calculations for the possible ReO_x species on the most dominant (110) alumina surface. Structure−reactivity relationships are developed for olefin metathesis of the supported ReO_x/Al_2O_3 catalysts by comparing the relationships between the initial surface ReO_x structures and their olefin metathesis reactivity.

2. RESULTS

2.1. In Situ UV−vis Spectroscopy. The in situ UV−vis edge energy (E_g) values for the dehydrated supported ReO_x/Al_2O_3 catalysts are presented in Figure 1 and exhibit a constant E_g value of ∼4.2 eV for all surface rhenia coverage (0.14−2.2 Re atoms/nm^2). The high UV−vis E_g value reflects the presence of only isolated surface rhenia species on alumina because the E_g values are comparable to those for the isolated ReO_4-containing

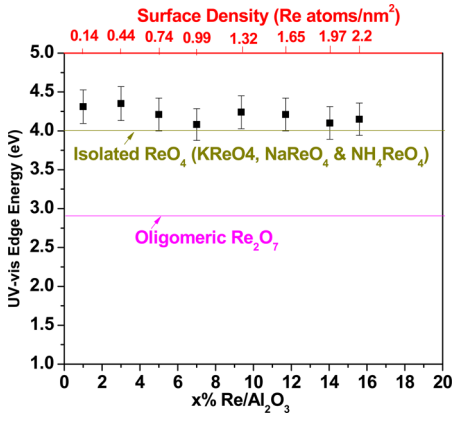

Figure 1. In situ UV−vis E_g values for dehydrated supported ReO_x/Al_2O_3 (Engelhard batch, E) catalysts as a function of rhenia surface coverage.

$NaReO_4$ (3.9 eV), $KReO_4$ (4.0 eV), and NH_4ReO_4 (4.0 eV) reference compounds and significantly higher than the E_g value for the oligomeric Re_2O_7 reference compound (2.8 eV) (see Figure S1). The absence of surface oligomeric and crystalline Re_2O_7 nanoparticles is a consequence of the volatility of dimeric and polymeric Re_2O_7 species, which assures that only isolated surface rhenia species are present on alumina.[5,6]

2.2. In Situ XANES and EXAFS Spectroscopies. The in situ XANES spectra of the supported ReO_x/Al_2O_3 catalysts under dehydrated conditions are shown in Figure 2.

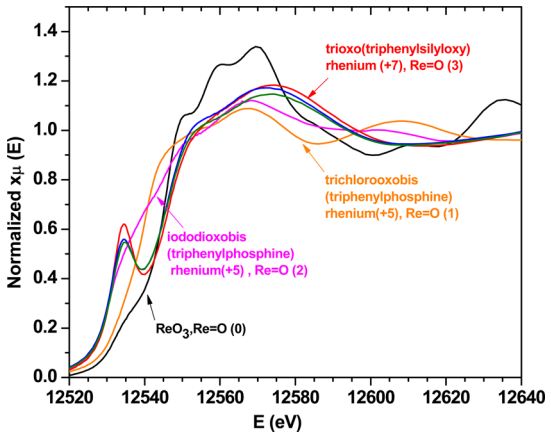

Figure 2. In situ Re L_1 XANES spectra for the dehydrated supported 3% (blue) and 15.6% (olive) ReO_x/Al_2O_3 catalysts. The XANES spectra of the reference compounds, trioxo(triphenylsilyloxy) rhenium(+7) (red), iododioxobis (triphenylphosphine) rhenium(+5) (magenta), trichlorooxobis (triphenylphosphine) rhenium(+5) (orange), and ReO_3 rhenium(+6) oxide (black) are taken under ambient conditions.

The coordination of the ReO_x site is reflected by the Re L_1 XANES pre-edge feature. For metal oxides with MO_6 coordination, O_h and inversion symmetry, the s−d transitions are dipole forbidden and, thus, there is no K or L_1 pre-edge.[17,18] Bulk ReO_3 possesses ReO_6 coordination (Figure S4), and the slight L_1 pre-edge is related to its minor distortion. Strong deviations from the MO_6 O_h symmetry result in a sharp pre-edge feature in the Re L_1 edge XANES reflecting the absence of inversion symmetry.[17] The trioxo(triphenylsilyloxy) rhenium (+7) reference compound consists of ReO_4 coordinated isolated $(O{=})_3$ReO-Si-(phenyl)$_3$ units containing C_{3v} symmetry (Figure S4) and exhibits a sharp Re L_1 XANES pre-edge because of the absence of inversion symmetry. The other rhenia reference compounds do not exhibit a strong Re L_1 XANES pre-edge. The in situ Re L_1 XANES spectra for the dehydrated supported 3% and 15.6% ReO_x/Al_2O_3 catalysts possess a strong pre-edge feature approaching that of the trioxo-(triphenylsilyloxy) Re^{7+} reference compound with C_{3v} symmetry. The slightly lower intensity of the pre-edge for the catalysts suggests that the ReO_x symmetry is slightly lower than C_{3v}, which may also be affected by some adsorption of residual moisture. The almost same XANES pre-edge intensity for both dehydrated supported ReO_x/Al_2O_3 catalysts also indicates that the surface ReO_x coordination does not change much with rhenia loading on the Al_2O_3 support.

The k^2 weighted Re L_1-edge EXAFS data of the corresponding samples are presented in Figure 3. The $(O{=})_3$ReO-Si-(phenyl)$_3$ reference compound with isolated rhenia sites exhibits a strong peak at ∼1.2 Å from the terminal

DOI: 10.1021/cs5016518
ACS Catal. 2015, 5, 1432−1444

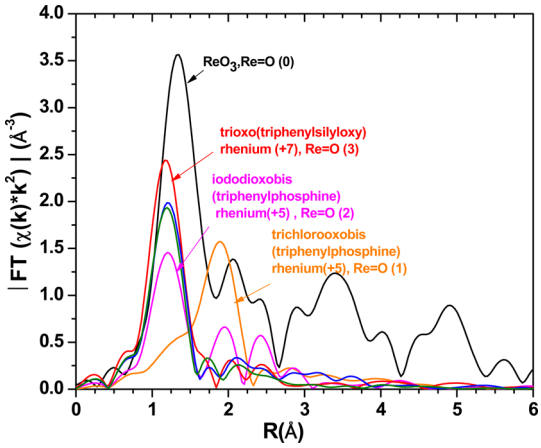

Figure 3. Magnitudes of Fourier-transformed, not-phase-corrected, k^2-weighted Re L_1-edge EXAFS spectra in the *R* space for the dehydrated supported 3%ReO_x/Al_2O_3 (blue) and 15.6%ReO_x/Al_2O_3 (olive) catalysts with the reference trioxo $(O{=})_3ReO\text{-}Si\text{-}(phenyl)_3$ (red), iododioxobis (triphenylphosphine) rhenium(+5) (magenta), trichlorooxobis (triphenylphosphine) rhenium(+5) (orange) and crystalline bulk ReO_3 (black) compounds.

Re=O bonds. The absence of strong peaks at high R distance is consistent with the isolated nature of the $(O{=})_3ReO\text{-}Si\text{-}(phenyl)_3$ reference compound. With the decrease in the number of Re=O bonds (3 in trioxo $(O{=})_3ReO\text{-}Si\text{-}(phenyl)_3$, 2 in iododioxobis (triphenylphosphine) rhenium, and 1 in trichlorooxobis (triphenylphosphine) rhenium), the intensity of the EXAFS peak at ~1.2 Å decreases. The crystalline bulk ReO_3 reference compound contains its Re−O peak at ~1.5 Å reflecting the longer metal−oxygen bond length in ReO_3 and absence of Re=O bonds in this structure. The bulk crystalline ReO_3 reference also possesses strong peaks in the 2−5 Å range, originating from the Re−Re single scattering path and several multiple scattering paths of this solid compound. The dehydrated supported ReO_x/Al_2O_3 catalysts have a pronounced peak at ~1.2 Å, similar to the location of the peak corresponding to Re=O bonds in the references. For both catalysts, the intensity of the peak at ~1.2 Å is almost the same and is between the intensities of the corresponding peaks in the standard compounds with 3 and 2 Re=O bonds. This type of change is consistent with the change of the number of Re=O pairs in the catalysts, and agrees well with the changes in the pre-edge peak of the corresponding XANES spectra. These two independent observations suggest that the catalysts possess mainly terminal Re=O bonds, and their coordination numbers can be estimated between 2 and 3 with symmetry less than C_{3v}. The absence of high R peaks in the spectra of catalysts reflects the isolated nature of the surface rhenia species on alumina, which is consistent with the above in situ UV−vis findings. Quantitative analysis yields the effective Re=O bond lengths of 1.72−1.75 Å for both species (Supporting Information (SI)). This is in agreement with the Re=O bond length values published in the recent literature,[12,13] but the actual number of Re=O bonds cannot be reliably obtained from EXAFS analysis because those contributions to EXAFS also correlate strongly with the single Re−O bonds at longer distances (e.g., 1.76 Å, as discussed later in the DFT section). The description of fitting models compared for the quantitative data analysis is presented in the SI.

2.3. In Situ Raman Spectroscopy. *2.3.1. Supported ReO_x/Al_2O_3 Catalysts under Dehydrated Conditions.* The in situ Raman spectra of the dehydrated supported ReO_x/Al_2O_3 catalysts are presented in Figure 4. The supported 3% ReO_x/Al_2O_3 catalyst, with a low surface rhenia coverage of 0.44 Re/nm^2, exhibits Raman bands at ~1002 ν_s(Re=O) (s), ~970 ν_{as}(Re=O) (w), ~879 ν_s(Re−O−Al) (m) and ~340 δ(O−Re−O) (m) cm^{-1} for the surface rhenia species (labeled ReO_x-I). Supported catalysts with 5% ReO_4 (≥0.74 Re/nm^2) and higher rhenia loading, as shown for 9.4% ReO_x/Al_2O_3 in Figure 4, possess a new ν_s(Re=O) (s) band at ~1012 cm^{-1} from a second surface rhenia species (labeled ReO_x-II) because each structure can only give rise to one symmetric stretch according to vibrational spectroscopy selection rules.[19] The surface ReO_x-II species possess vibrations at 1012 ν_s(Re=O) (s), ~976 ν_{as}(Re=O) (w), ~890 ν_s(Re−O−Al) (m), and ~340 δ(O−Re−O) (m) cm^{-1}. The absence of vibrations from bending δ_s(Re−O−Re) (m) at ~150−250 cm^{-1}, stretching ν_s(Re−O−Re) (w) at ~400−600 cm^{-1} and stretching ν_{as}(Re−O−Re) (vw) at ~600−800 cm^{-1} (see SI, Figure S7 for the Raman spectrum of solid Re_2O_7) is further consistent with the isolated nature of the surface ReO_x species on alumina.[5,6]

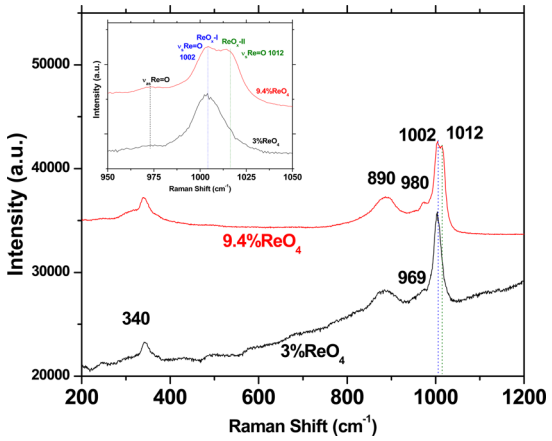

Figure 4. In situ Raman spectra (442 nm) of dehydrated supported 3% and 9.4% ReO_x/Al_2O_3 (Harshaw batch, H) catalysts at 100 °C. The inset shows the 900−1100 cm^{-1} region.

2.3.2. Supported $ReO_x/TaOx/Al_2O_3$ under Dehydrated Conditions. The simultaneous presence of two dehydrated surface ReO_x species at high surface rhenia coverage on alumina greatly complicates molecular structural analysis of the surface ReO_x-II site. To resolve this problem, we chose to use a second surface metal oxide that may behave similarly to surface ReO_x-I and does not give rise to strong Raman bands that would interfere with the rhenia vibrations (the motivation for this strategy is given below in section 3.4.2). Surface TaO_x was selected as the second metal oxide because previous studies showed that the supported TaO_x/Al_2O_3 system does not give strong Raman bands (as shown in SI, Figure S8 for 15% Ta_2O_5/Al_2O_3, which is about half a monolayer of surface TaO_x on alumina).[20] The influence of the secondary surface TaO_x species on the supported ReO_x/Al_2O_3 catalyst system is also shown in SI, Figure S8, and only the Raman vibrations corresponding to the surface ReO_x-II species on alumina are found at ~1010 ν_s(Re=O) (s), ~980 ν_{as}(Re=O) (w), 890 ν_s(Re−O−Al) (m) and 345 δ(O−Re−O) (m) cm^{-1}.[5,6] The order of impregnation and calcination of TaO_x or ReO_x does not affect the final results (compare ReTaAl and TaReAl spectra in SI, Figure S8) suggesting that surface TaO_x is able to

DOI: 10.1021/cs5016518
ACS Catal. 2015, 5, 1432−1444

block formation surface ReO_x-I species and, thus, increase the number of surface ReO_x-II sites. This is *the first time* that the surface ReO_x-II species have been successfully isolated on the alumina support.

2.3.3. Isotopic $^{16}O-^{18}O$ Exchange of Supported ReO_x/Al_2O_3 Catalysts. Time-resolved in situ Raman spectroscopy isotopic $^{18}O-^{16}O$ exchange studies were undertaken with $H_2{}^{18}O$ to assist in the discrimination between surface trioxo $(O=)_3ReO_x$, dioxo $(O=)_2ReO_x$, and mono-oxo $O=ReO_x$ species on alumina. During isotopic oxygen exchange, (*i*) trioxo species are expected to split into four Raman bands ($(=^{16}O)_3$, $(=^{16}O)_2(=^{18}O)$, $(=^{16}O)(=^{18}O)_2$ and $(=^{18}O)_3$), dioxo species should split into three Raman bands ($(=^{16}O)_2$, $(=^{16}O)(=^{18}O)$ and $(=^{18}O)_2$), and mono-oxo species will split into two Raman bands ($(=O^{16})$ and $(=O^{18})$).

The time-resolved isotopic oxygen exchange Raman spectra for the supported 3% ReO_x/Al_2O_3 (H) catalyst that only possesses the surface ReO_x-I species are presented in Figure 5.

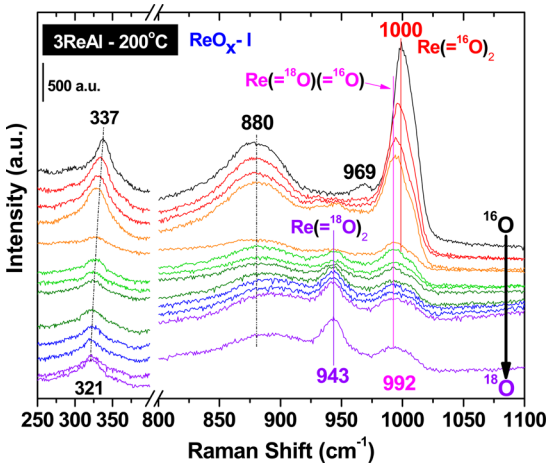

Figure 5. In situ Raman spectra (442 nm) of 3% ReO_x/Al_2O_3 (ReO_x-I) (H) at 200 °C during $^{18}O-^{16}O$ isotope exchange by exposure to $H_2{}^{18}O$ vapor.

The time-resolved Raman spectra indicate three ν_s(Re=O) vibrations that are only consistent with dioxo surface ReO_x species at ~1000 ($^{16}O=Re=^{16}O$), 992 ($^{18}O=Re=^{16}O$) and 943 cm^{-1} ($^{18}O=Re=^{18}O$). The corresponding δ(O–Re–O) mode shifts from 337 to 321 cm^{-1} during the isotopic exchange process while the broad ν_s(Re–O–Al) band at 880 cm^{-1} and weak ν_{as}(Re(=O) band at 969 cm^{-1} stretching vibrations become too weak to detect.

The time-resolved isotopic oxygen exchange Raman spectra for the supported 10% ReO_x/10% Ta_2O_5/Al_2O_3 (E) catalyst that only possesses the surface ReO_x-II species are presented in Figure 6. The time-resolved Raman spectra indicate three ν_s(Re=O) vibrations that are only consistent with dioxo surface ReO_x species at ~1010 ($^{16}O=Re=^{16}O$), 995 ($^{18}O=Re=^{16}O$) and 950 cm^{-1} ($^{18}O=Re=^{18}O$). The corresponding δ(O–Re–O) mode shifts from 345 to 327 cm^{-1} during the isotopic exchange, whereas the broad ν_s(Re–O–Al) band at 897 cm^{-1} and the very weak ν_{as}(Re(=O) band at ~980 cm^{-1} become too weak to detect with the isotopic oxygen exchange.

2.4. In Situ IR Spectroscopy under Dehydrated Conditions. *2.4.1. Overtone Region.* The strong absorption of the IR radiation by the Al_2O_3 support prevents observation of the Re=O and Re–O vibrations in the fundamental

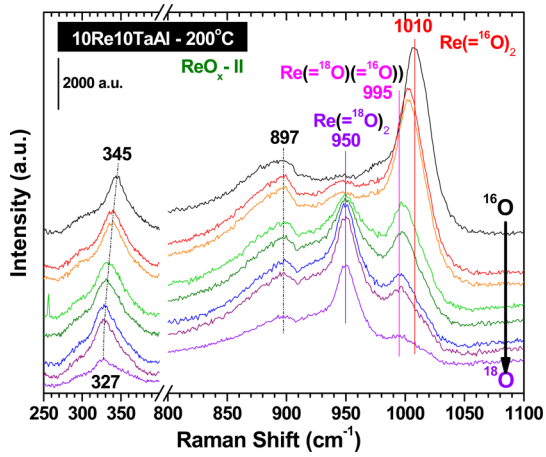

Figure 6. In situ Raman spectra (442 nm) of supported 9.36% ReO_x/10%Ta_2O_5/Al_2O_3 (ReO_x-II) (E) at 200 °C during $^{18}O-^{16}O$ isotope exchange with $H_2{}^{18}O$ vapor.

frequency region (~1000 cm^{-1} and below). The Re=O vibrations, however, can be observed in the overtone region and the in situ IR spectra of the dehydrated supported ReO_x/Al_2O_3 catalysts in the overtone region are shown in SI, Figure S9. The supported 3% ReO_x/Al_2O_3 catalyst that only contains the surface ReO_x-I species gives rise to two broad bands in the overtone region at ~1996 (s) and ~1962 (s) cm^{-1} from the ν_s(Re=O) and ν_{as}(Re=O) vibrations, respectively. At higher surface rhenia coverage, two additional shoulders appear at ~2020 (m) and ~1971 (m) cm^{-1} are also present from the ν_s(Re=O) and ν_{as}(Re=O) vibrations of the surface ReO_x-II species, respectively. These observations and assignments are in agreement with prior IR studies of supported ReO_x/Al_2O_3 catalysts and further support the presence of two distinct surface ReO_x species on alumina.[6] The IR bands, however, are very broad and significantly overlap compared to the sharper Raman bands, which makes Raman the preferred method to monitor the surface ReO_x species on alumina.

2.4.2. Surface Hydroxyl (OH) Groups. 2.4.2.1. Supported ReO_x/Al_2O_3 Catalysts under Dehydrated Conditions. The alumina surface hydroxyls of under dehydrated conditions have been extensively studied in the catalysis literature and at least 5 types of surface hydroxyls are present and their coordination to the different surface alumina sites are given in Table 1.[15,16,21,22]

Table 1. Al_2O_3 hydroxyl types and band positions (cm^{-1}) reported in the literature

band positions	crystal faces[15,16]	structure of hydroxyl sites (from DFT)[15,16]
3785–3800	(110)	HO-μ_1-Al_{IV}
3760–3780	(100)	HO- μ_1-Al_{VI}
3730–3735	(110)	HO-μ_1-Al_V
3690–3710	(110)	HO-μ_2-Al_V
3590–3650	(100)	HO-μ_3-Al_{VI}

The in situ IR spectra of the surface hydroxyl region of the dehydrated supported ReO_x/Al_2O_3 catalysts as a function of rhenia loading are presented in Figure 7. At low surface ReO_x coverage (3% ReO_x/Al_2O_3), mainly the μ_1-Al_{IV}, μ_1-Al_{VI} and μ_1-Al_V surface hydroxyls at 3787, 3768, and 3743 cm^{-1}, respectively, are consumed due to anchoring of the surface rhenia species on alumina. Minor amounts of μ_3- Al_{VI} surface

DOI: 10.1021/cs5016518
ACS Catal. 2015, 5, 1432–1444

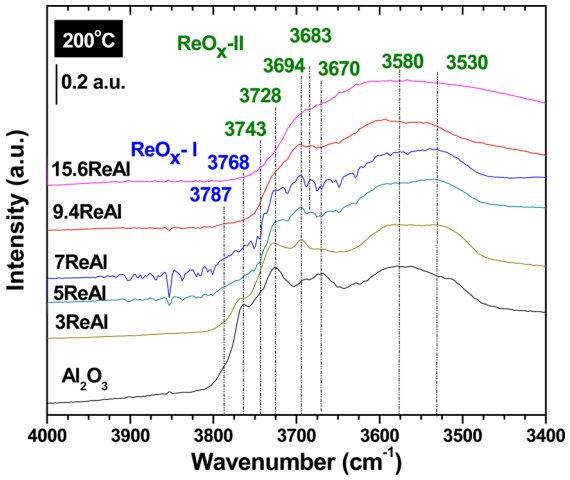

Figure 7. In situ IR spectra of the surface hydroxyl region of dehydrated supported ReO_x/Al_2O_3 (E) catalysts as a function of rhenia loading at 200 °C. The blue color represents ReOx-I, and the green color represents ReOx-II.

hydroxyls at 3670 cm^{-1} also appear to be consumed. At intermediate surface ReO_4 coverage (9.4% ReO_x/Al_2O_3), the consumption of the μ_1-Al_V hydroxyl at 3728 cm^{-1} becomes significant, the 3694 cm^{-1} μ_2-Al_V hydroxyl are only slightly consumed and there does not appear to be any significant amount of μ_1 surface hydroxyls (3730−3800 cm^{-1}) remaining. At the highest surface ReO_x coverage (15.6% ReO_x/Al_2O_3), almost all of the IR observable alumina surface hydroxyls have been consumed. There is no indication for the formation of Re−OH hydroxyls under the dehydrated conditions. The in situ IR spectra reveal that different alumina surface hydroxyls are employed in anchoring the surface ReO_x species on the alumina support and explain why more than one surface ReO_x species is present on the alumina support with rhenia coverage.

2.4.2.1. Supported $ReO_x/Ta_2O_5/Al_2O_3$ Catalysts. The surface TaO_x species anchor at the same basic surface hydroxyl sites consumed by surface ReO_x-I species (see SI, Figure S10). Consequently, the surface rhenia species can only anchor at the surface hydroxyl sites available for forming surface ReO_x-II species.

2.5. In Situ Raman Spectroscopy during Propylene Metathesis. In situ Raman spectra were also collected during propylene metathesis (1% C_3=/He at 70 °C), and the spectra for the supported 3%ReO_x/Al_2O_3 (H), 9.4%ReO_x/Al_2O_3 (H) and 5%ReO_x/15%TaO_x/Al_2O_3 (E) are presented in panels a, b, and c, respectively, of Figure 8. The surface ReO_x-I species (~1003 cm^{-1}) are minimally perturbed by the reaction environment, only decreasing its Raman intensity by ~3−7% up to 120 min as shown in Figure 8a,b. The surface ReO_x-II species (~1011 cm^{-1}), however, clearly undergo preferential interaction with propylene over the surface ReO_x-I species during propylene metathesis, as shown in Figure 8c. The strong interaction of propylene with the surface ReO_x-II sites, formed by addition of 15% TaO_x to 5% ReO_x/Al_2O_3 that suppresses formation of surface ReO_x-I sites, is clearly indicated in Figure 8c, as the intensity of the Raman band is almost completely diminished after 120 min of reaction. Recovery of the initial surface ReO_x Raman bands after reaction by reoxidation of the catalysts indicates that the decreased Raman intensity during propylene metathesis was not caused by volatilization of surface rhenia from the catalyst.

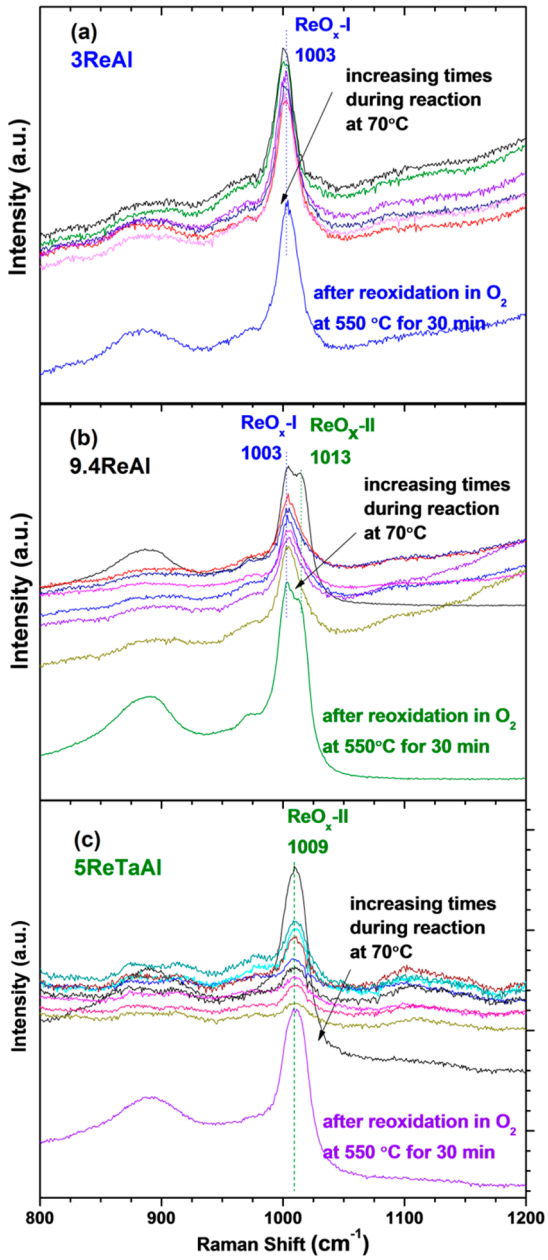

Figure 8. In situ Raman spectra (442 nm) of the (a) 3%ReO_x/Al_2O_3 (H), (b) 9.4%ReO_x/Al_2O_3 (H), and (c) 5%ReO_x/15%TaO_x/Al_2O_3 (E) catalysts during propylene metathesis at 70 °C up to 120 min. The catalyst was reoxidized in 10% O_2/Ar at 550 °C after the reaction.

2.6. Density Functional Theory Calculations. *2.6.1. Surface ReO_x Structures on the Al_2O_3 Support.* Comparison of the adsorption energy of a model $HReO_4$ compound shows that the Al_2O_3(110) termination has a higher reactivity toward the surface ReO_x species compared to the more stable Al_2O_3(100) facet (see SI). This is a general feature for many Lewis base molecules and is related to the presence at the (110) surface of low coordinated Al_{III} and Al_{IV} sites, which present efficient acceptor orbitals of low energy (especially the Al_{III} site), whereas the (100) termination show less reactive Al_V surface atoms.[23] Hence occupation of the Al_2O_3(110) surface by the ReO_x species is most probable, and the DFT calculations below will be limited to the Al_2O_3(110) facet. An extensive discussion of the DFT calculations of surface ReO_x species on the less reactive Al_2O_3(100) surface can be found in SI (Figure

DOI: 10.1021/cs5016518
ACS Catal. 2015, 5, 1432−1444

S2). The Al_{III} sites result from the truncation at the (110) surface of tetra-coordinated Al atoms that are specific to the γ-alumina structure and are absent in α-alumina. The calculations here are performed in the limit of low hydroxyl content of the surface, however, at moderate hydration level accessible metastable structures with strong Lewis acid are also seen on the (110) alumina surface.[24]

The supported rhenia structures obtained for the majority (110) γ-alumina surface are shown in Figure 9.

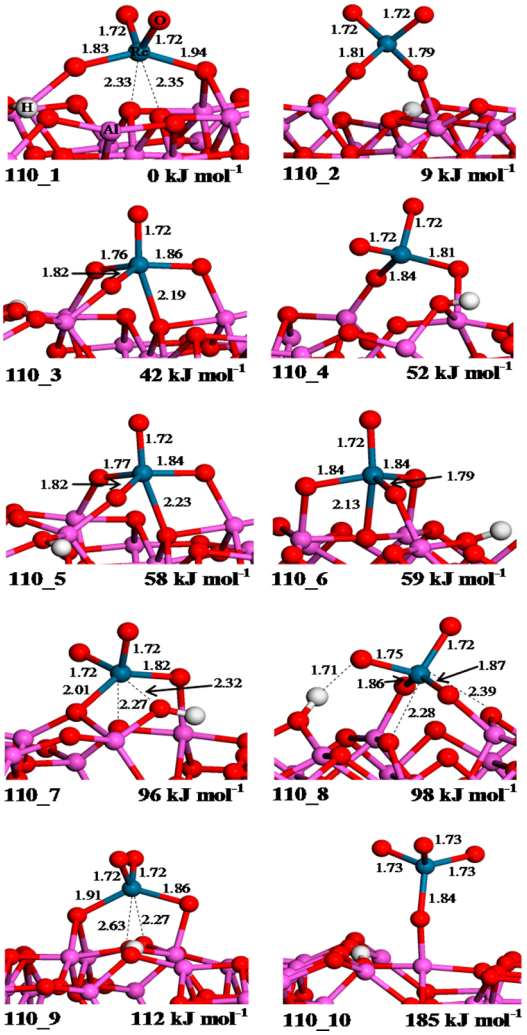

Figure 9. DFT optimized structures and relative energies for the surface Re^{7+} oxide species supported on (110) γ-alumina. Bond lengths are given in Å.

The optimized rhenia structures obtained for the (110) γ-alumina surface are especially important because this is the most exposed surface on alumina nanoparticles and is also more unsaturated; consequently, it is more reactive than the (100) surface.[15,16] This produces a larger variety of surface rhenium oxide species compared to the (100) plane, and the surface rhenium oxide species are also more strongly bonded to the alumina support. The optimized ReO_x structures in Figure 9 possess trioxo, dioxo, and mono-oxo rhenium oxide coordination. The predicted Re═O bond lengths for the free Re═O bonds are typically 1.72 Å for the mono-oxo and dioxo structures, and 1.73 Å for the trioxo species 110_10, again in accordance with the EXAFS results.[12,13] An interaction between the oxo ligand and surface hydroxyl group causes an elongation of the double bond to 1.75 Å (110_8). The formally single Re−O bonds involved in Re−O−Al linkages are nonequivalent with their lengths varying over a wide range from 1.76 to 2.01 Å.

The relative energies of the obtained structures sometimes differ dramatically. The trioxo species with the C_{3v} symmetry (110_10) is clearly predicted to be unstable, and other attempts to obtain trioxo Re^{7+} structures resulted in dioxo species. The formation of mono-oxo Re^{7+} species was also considered (110_3, 110_5, and 110_6) because of the high reactivity of the alumina surface. Each of the rhenium mono-oxo structures is 4-fold bonded to the alumina surface with three bridging Re−O−Al bonds and one additional dative bond from a surface oxygen atom to the rhenium atom. The most stable structures, however, are the surface dioxo species (110_1 and 110_2). Although they are very close in energies, their geometries are not identical. For the 110_1 structure, the ReO_4 unit is strongly deformed toward a C_{2v} symmetry with two additional weak and long Re···O bonds (2.35 Å) forming with surface O atoms. Such interactions, where the Re atom plays the role of a Lewis acid, complete the Re coordination and only form on the Al_2O_3 (110) surface because they require more basic oxygen atoms. There are two bridging oxygen atoms in this species, connected to one AlO_4 and two AlO_5 aluminum atoms, respectively (here we refer to the final coordination of these Al atoms after interaction with Re). The surface 110_2 species appears as a ReO_4 coordinated unit. The rhenium atom is connected via two oxygen bridges with one AlO_4 and one AlO_5 site. The surface rhenia structures obtained here, stabilized by multiple interactions with the surface, are consistent with earlier computational study on methyltrioxorhenium adsorbed on (110) γ−Al_2O_3.[23] A detailed discussion concerning the stability of the surface rhenium species in terms of deformation and interaction energy is included in SI.

The present DFT optimization study with realistic alumina surface models strongly supports the proposal that surface rhenium oxide species on γ-alumina exhibit a dioxo ReO_4 structure and do not reproduce the proposed penta-coordinated dioxo Re species.[13] Because this (110) termination shows two structures with very similar energy, calculations suggest that the supported catalyst may be a mixture of different binding modes of the ReO_4 on γ-alumina, most likely having the surface (110_1) and (110_2) structures. It should, however, be noted that species of similar geometry can significantly differ in their stability, depending on their specific location on the surface (for instance, compare 110_1 and 110_9). Hence, surface stability of the ReO_x species might be strongly dependent on the detailed geometry of the alumina surface. The presence of defects or of different levels of hydration may also affect the complex geometry and stability.[24] Additional information is, thus, mandatory to confirm the trend proposed by the energy calculations.

2.6.2. Predicted Raman Vibrations from DFT Calculations. A key link with experiment is established by the calculation of vibrational frequencies. A benchmark study of Re═O frequencies with a well-characterized family of gas phase rhenium oxide compounds (data obtained from literature[25−28]) indicates that for optimum accuracy, a scale factor of 0.9900 needs to be applied (Table 2). Note that the correction with respect to raw calculated data is small. The very good agreement between theoretical and experimental values is another validation of the adopted methodology in this study.

DOI: 10.1021/cs5016518
ACS Catal. 2015, 5, 1432−1444

Table 2. Calculated and Experimental Re=O Stretching Frequencies (cm^{-1}) for Reference Rhenium Oxide Reference Compounds, after the Determination of the Optimum Scaling Factor of 0.9900

	calcd[a]		exptl	
	ν_s(Re=O)	ν_{as}(Re=O)	ν_s(Re=O)	ν_{as}(Re=O)
$Re_2O_{7(g)}$	1006	975	1008[b]	975[b]
$HReO_{4(g)}$	1000	973	-	972[b]
$ReO_3F_{(g)}$	1011	979	1013[c]	978[c]
$CH_3ReO_{3(g)}$	1000	974	1003[d]	975[d]
$ReO_{2(g)}$	984	936	981–984[e]	931–934[e]

[a]A scale factor of 0.9900 is used. [b]ref 25. [c]ref 26. [d]ref 27. [e]ref 28.

The calculated Raman vibrations of each of the supported ReO_x structures on the alumina surface are presented in SI, Table S1. It should be noted that Re=O and Re−O−Al vibrations are often coupled to each other. Furthermore, the vibrations of the mono-oxo, dioxo, and trioxo surface ReO_x structures overlap, and it is not possible to discriminate between the different structures on the positions of the bands alone. For example, all the surface ReO_x structures on the Al_2O_3(100) surface exhibit their strong ν_s (Re=O) stretch in the narrow region: between 987 and 997 cm^{-1} and on the Al_2O_3(110) surface mono-oxo 110_3 and 110_5 (996 and 992 cm^{-1}), dioxo 110_7 (990 cm^{-1}), and trioxo 110_10 (997 cm^{-1}) are too close to be able to distinguish between them.

Isotopic oxygen exchange studies give key additional information in order to discriminate between mono-oxo, dioxo, and trioxo surface ReO_x species on the most dominant Al_2O_3(110) surface as shown experimentally above with Raman spectroscopy. The calculated isotopic $^{18}O-^{16}O$ shifts in the Re=O stretching frequencies for the most stable dioxo Re species on the (110) γ-alumina surface (110_1 and 110_2) are shown in Table 3. Additionally, the theoretical frequencies for the mono-oxo (110_3) and trioxo (110_10) Re models after the isotopic exchange are also presented. In the calculations, the $^{18}O-^{16}O$ substitution has been considered only for the oxo ligands (Re=O bonds) that dominate these vibrations. In the case of the partially substituted dioxo and trioxo species, all possible substitution patterns are taken into account for the determination of the theoretical frequencies. The calculated Re(=^{18}O)(=^{16}O), Re(=^{18}O)(=^{16}O)$_2$, and Re(=^{18}O)$_2$(=^{16}O) frequencies hardly depend on the substitution sequence. In most cases, the Re=O stretching modes are coupled with the Re−O−Al vibrations.

The calculated isotopic shifts for the 110_1 and 110_2 dioxo surface ReO_4 species are consistent with the experimental data for the supported ReO_x/Al_2O_3 catalysts (Table 4), especially for the symmetric Re=O modes. The theoretically predicted frequencies for the fully substituted trioxo Re species (962, 922, and 915 cm^{-1} in Table 3) are different from the corresponding experimental values assigned to the species ReO_x-I and ReO_x-II (950–942 cm^{-1} in Table 4), confirming that surface ReO_x species are not trioxo. The calculated ν_s(Re=^{16}O) (996 cm^{-1}) and ν_{as} (Re=^{18}O) (945 cm^{-1}) frequencies for the mono-oxo species 110_3 (Table 4) are close to the observed bands of the symmetric modes for the nonsubstituted (1000 cm^{-1}) and fully substituted (943 cm^{-1}) species ReO_x-I, respectively (Table 4). However, in contrast to (110_1), the mono-oxo ReO_x species does not match all the observed bands and its existence is not confirmed experimentally. Such mono-oxo species as (110_3) cannot entirely be excluded as minority species by the DFT

Table 3. Effect of the Isotopic $^{18}O-^{16}O$ Exchange on the Calculated[a] Re=O Stretching Frequencies (cm^{-1}) for the Rhenium Oxide Species Supported on the γ-Alumina Surface

110_3 (monooxo)	sites	110_1 (dioxo)	110_2 (dioxo)	sites	110_10 (trioxo)	sites
996	ν(Re=^{16}O)	1003	1014	ν_s(Re(=^{16}O)$_2$)	997	ν_s(Re(=^{16}O)$_3$)
945	ν(Re=^{18}O)	992–991	1004–1001	ν_s(Re(=^{18}O)(=^{16}O))	991–989	ν_s(Re(=^{18}O)(=^{16}O)$_2$)
		952	967	ν_s(Re(=^{18}O)$_2$)	981–978	ν_s(Re(=^{18}O)$_2$(=^{16}O))
		976	985	ν_{as}(Re(=^{16}O)$_2$)	962[d], 922, 915	ν_s(Re(=^{18}O)$_3$)
		938–937, 915[b]	953–950, 937–935[b]	ν_{as}(Re(=^{18}O)(=^{16}O))	956–955	ν_{as}(Re(=^{16}O)$_3$)
		927	939[c], 933	ν_{as}(Re(=^{18}O)$_2$)	957–955, 942–940[d], 912–909	ν_{as}(Re(=^{18}O)(=^{16}O)$_2$)
					946–942, 918, 914–913[b], 907–906	ν_{as}(Re(=^{18}O)$_2$(=^{16}O))
					908–906	ν_{as}(Re(=^{18}O)$_3$)

[a]A scale factor of 0.9900 is used. [b]Strongly coupled with ν(Re−O−Al). [c]ν(O=Re−O−Al) coupled with ν(Al−O−Re−O-Al). [d]ν(Re−O−Al) coupled with ν((Re=O)$_3$).

DOI: 10.1021/cs5016518
ACS Catal. 2015, 5, 1432–1444

Table 4. Comparison of DFT Calculated Re=O Stretching Frequencies for the Surface Dioxo ReO_x Species with Experimentally Measured Re=O Vibrations for Supported ReO_x/Al_2O_3 Catalysts

DFT (110_1)	exptl (ReO_x-I)	sites	DFT (110_2)	exptl (ReO_x-II)	sites
1003	1000	$\nu_s(Re(=^{16}O)_2)$	1014	1010	$\nu_s(Re(=^{16}O)_2)$
992–991	992	$\nu_s(Re(=^{18}O)(=^{16}O))$	1004–1001	995	$\nu_s(Re(=^{18}O)(=^{16}O))$
952	946–942	$\nu_s(Re(=^{18}O)_2)$	967	950	$\nu_s(Re(=^{18}O)_2)$
976	970	$\nu_{as}(Re(=^{16}O)_2)$	985	980	$\nu_{as}(Re(=^{16}O)_2)$
938–937, 915[a]		$\nu_{as}(Re(=^{18}O)(=^{16}O))$	953–950, 937–935[a]		$\nu_{as}(Re(=^{18}O)(=^{16}O))$
927	915[c]	$\nu_{as}(Re(=^{18}O)_2)$	939[b], 933	915[c]	$\nu_{as}(Re(=^{18}O)_2)$

[a]Strongly coupled with ν(Re–O–Al). [b]ν(O=Re–O–Al) coupled with ν(Al–O–Re–O-Al). [c]It was not possible to isolate and assign this vibration to an individual species.

calculations because their vibrational stretching modes may be screened by the symmetric vibrations of the major dioxo species. Therefore, the combination of total energy calculations and of frequency calculations including isotopic exchange show that the two most energetically favored species on the most dominant 110 planes, 110_1 and 110_2, are observed experimentally as surface ReO_4–I and ReO_4–II, respectively.

2.7. Steady-State Propylene Metathesis. The steady-state catalytic performance of the supported ReO_x/Al_2O_3 catalysts for propylene metathesis to ethylene and 2-butene is shown in Figure 10. The same trend is also obtained

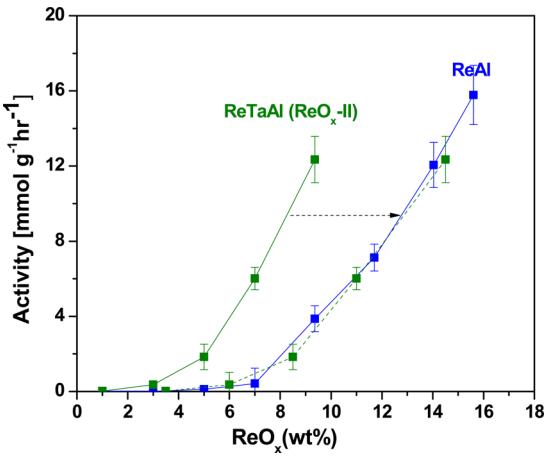

Figure 10. Steady-state catalytic performance for propylene metathesis at 70 °C by supported ReO_x/Al_2O_3 (blue squares) and ReO_x/%15% TaO_x/Al_2O_3 (green squares) catalysts that were dehydrated in flowing O_2/Ar at 500 °C for prior to reaction at 70 °C. The reaction was performed with ReO_x catalysts supported on Al_2O_3 (E). The dashed line indicates the *x*-axis shift for ReTaAl catalysts to show the promotion effect of the surface TaO_x species. The slight offset may be due to experimental error such as volatilization of ReO_x at higher loading.

independent of the activity normalization (g of catalyst or m^2 because all the catalysts possess similar BET values). For the supported ReO_x/Al_2O_3 catalyst, there is almost no propylene metathesis activity below ~5% ReO_x/Al_2O_3 (0.74 Re/nm^2) loading, and the metathesis activity increases continuously only with ReO_x loading above ~5% ReO_x (0.74 Re/nm^2). Comparison of the propylene metathesis activity with the surface ReO_x-I and ReO_x-II structures on alumina determined above suggests that the surface ReO_x–I sites possess minimal activity for metathesis. Although the Ta_2O_5/Al_2O_3 support is not active for propylene metathesis, the addition of surface TaO_x species significantly promotes the activity of supported ReO_x/Al_2O_3 catalyst by increasing the propylene metathesis at all surface rhenia coverage on alumina (e.g., by a factor of ~10× for 3% ReO_x and ~4× for 9.4% ReO_x). Furthermore, it appears that the surface TaO_x species only replace the surface ReO_x-I sites because the $ReO_x/TaO_x/Al_2O_3$ activity curve matches the activity of ReO_x/Al_2O_3 by shifting the curve to higher rhenia loadings as shown by the dashed line in Figure 10. This suggests that the surface TaO_x sites on alumina do not participate in the propylene metathesis reaction.

3. DISCUSSION

3.1. Molecular Structures and Anchoring Sites of the Surface ReO_x Species on Al_2O_3. Only isolated surface ReO_x species are present on the alumina support because dimeric Re_2O_7 or higher rhenia oligomers are volatile. This is the reason for the volatilization of rhenia from alumina at high surface rhenia coverage.[5,6] The isolated nature of the surface ReO_x site on alumina is supported by the very high UV–vis E_g values and the absence of observable Re–Re distances in the second coordination sphere at ~3–4 Å in the EXAFS radial distribution of the dehydrated supported ReO_x/Al_2O_3 catalysts.[12,13] TOF-SIMS analysis of calcined supported ReO_x/Al_2O_3 catalysts also demonstrated that the surface ReO_x species are essentially isolated on the alumina support.[29]

The intense Re L_1 XANES pre-edge feature of the supported ReO_x/Al_2O_3 catalysts approaches that of the $(O=)_3$ReO-Si-$(phenyl)_3$ reference compound in (see Figure 2), which strongly suggests that the surface ReO_x sites possess ReO_4 coordinated with only slightly different symmetry than C_{3v} from the reference compound. The presence of the two long Re···O bonds (2.35 Å) bonds for the deformed (110_1) surface ReO_4 structure does not appear to influence its first coordination shell and, thus, its XANES pre-edge features. Structures with other symmetries such ReO_6 or ReO_5 would give rise to very weak or intermediate XANES Re L_1 pre-edges, respectively. The somewhat weaker Re=O peak in the Re L_1 EXAFS of the dehydrated supported ReO_x/Al_2O_3 relative to the trioxo $(O=)_3$ReO-Si-$(phenyl)_3$ reference compound suggests less Re=O character and more Re–O character for the surface ReO_4 sites on the Al_2O_3 support. The isotopic $^{18}O-^{16}O$ oxygen exchange measurements confirm that the surface ReO_4 sites contain two oxo ligands (O=Re=O) (see Figure 5). This molecular structure is also supported by the DFT calculations indicating that the most stable surface rhenia structures on alumina are dioxo surface ReO_4 species. Moreover, spectroscopy and theory demonstrate that two distinct dioxo species are present. Dioxo surface ReO_4–I is assigned to the 110_1 in Figure 9, where, besides the two Re=O bonds, there are also two bridging Re–O–Al bonds and two much longer Re---O-Al bonds to the support, with the latter outside of the first coordination sphere of the surface ReO_4–I

DOI: 10.1021/cs5016518
ACS Catal. 2015, 5, 1432–1444

site. The dioxo surface ReO_4−II is assigned to the slightly less stable DFT-calculated structure 110_2 in Figure 9 with two oxo bonds (O═Re═O) and two longer bridging Re−O−Al bonds. For the Re═O vibrational stretch frequencies, DFT calculations also predict the observed isotopic shift from ∼1003/976 to ∼1014/985 cm^{-1} for the surface ReO_4−I and ReO_4−II sites, respectively, on the alumina (110) surface (see Table 4).

The slight structural differences between the surface ReO_4−I and ReO_4−II sites is directly related to the bridging Re−O−Al bonds (1.83/1.94 Å and 1.79/1.81 Å on the Al_2O_3 (110) surface, respectively) and to an angular distortion of the tetrahedral Re center in ReO_4−I, because both rhenia sites have the same Re═O bond lengths of 1.72 Å. The surface ReO_4−I site on alumina (110) is connected to one Al_{IV} site and two Al_V sites, in agreement with the observed preferential consumption of basic alumina μ_1 surface hydroxyls for 1−5% ReO_4/Al_2O_3 in the IR spectra (see Figure 7). The surface ReO_4−I site requires Lewis acid Al sites and additional surface basic O atoms for its stabilization on the alumina (110) surface. In the DFT model (110_2), the ReO_4 species is supported by a vacant alumina surface and hence is a metastable case. In the experiment, surface ReO_4−II only appears after a loading of 5% and hence is anchored at μ_2-Al_{VI} and μ_3-Al_{VI} sites in agreement with the observed preferential consumption of the corresponding μ_2-Al_V and μ_3-Al_{VI} surface hydroxyls on alumina (110) for 5−15.6% ReO_4/Al_2O_3 (see Figure 7). The impregnation of Ta_2O_5 consumes Al_{IV} and Al_V sites, which are involved in anchoring surface ReO_4−I species and, hence, only allows selective formation of surface ReO_x-II at low Re loading (see SI, Figure S10). Regardless of the order of impregnation, the surface ReO_4−II species are always dominant on the Al_2O_3 support in the presence of Ta_2O_5 due to the higher mobility of surface ReO_x species.

As seen above, the most stable surface ReO_x sites on Al_2O_3 are the surface dioxo $(O═)_2ReO_2$ sites as predicted by DFT calculations based on the stability of different surface ReO_x structures on realistic models of the Al_2O_3 surface and confirmed experimentally with in situ XANES and isotopic $^{18}O-^{16}O$ exchange Raman spectroscopy. The current DFT optimizations do not reproduce the proposed penta-coordinated dioxo $(O═)_2ReO_3$ species as a stable surface ReO_x structure.[13] The most common proposed structure in the literature for surface ReO_x sites on alumina has been the trioxo $(O═)_3Re-O-Al$ structure.[5−12] The $^{18}O-^{16}O$ exchange Raman findings are not consistent with trioxo species and the DFT calculations clearly indicate that the trioxo ReO_4 structure is not stable on the alumina (110) surface. The formation of mono-oxo $O═ReO_4$ species was also considered (see structures 110_3, 110_5, and 110_6 in Figure 9), but the presence of mono-oxo $O═ReO_4$ species is also not supported by the $^{18}O-^{16}O$ exchange findings and DFT calculations predict the mono-oxo ReO_x structure to be less stable than dioxo on the alumina (110) surface. The two previous structural assignments of surface trioxo $(O═)_3ReO$ and penta-coordinated dioxo $(O═)_2ReO_3$ were based on fitting of the EXAFS radial distributions of the oxygen atoms surrounding the Re^{7+} site.[12,13] The current EXAFS analysis indicates that it is not possible to determine the exact number of Re═O bonds with EXAFS alone since both the Re═O and Re−O bonds have similar bond lengths that complicates analysis. In addition, EXAFS analysis, which averages over the two surface ReO_4 sites on Al_2O_3, further complicates molecular structural analysis. Although the surface dioxo $(O═)_2ReO_2$ structure has previously not been proposed in the literature, the current experimental and theoretical calculations strongly indicate that it is the stable surface rhenia species on dehydrated supported ReO_x/Al_2O_3 catalysts.

3.2. Influence of the Propylene Metathesis Reaction Conditions on the Surface ReO_4−I and ReO_4−II Sites on Al_2O_3. The in situ Raman studies of the supported ReO_4/Al_2O_3 catalysts (3% ReO_4/Al_2O_3 with only surface ReO_4−I sites, 15.6% ReO_4/Al_2O_3 with both surface ReO_4−I and surface ReO_4−II sites, and 3% ReO_4/15% TaO_x/Al_2O_3 with only surface ReO_4−II sites) during propylene metathesis clearly demonstrate that the surface ReO_4−I sites are minimally perturbed by propylene and that all the surface ReO_4−II sites readily interact with propylene (see panels a, b, and c, respectively, of Figure 8). The nature of the surface ReO_x-II sites interacting with propylene is the subject of a subsequent study and will not be currently addressed.

The interaction of all the surface ReO_4−II sites on Al_2O_3 with propylene is unexpected because the olefin metathesis literature has been under the impression that only a very small number of sites, ∼1% ReO_4, are active sites for metathesis.[29] This conclusion was reached from olefin metathesis titration studies at ambient temperatures (25−50 °C). The titration measurements were conducted at ambient temperatures after several hours of olefin metathesis and exposing the catalyst to vacuum for several hours to remove residual physically adsorbed olefins from the catalysts before titration with a second olefin. The presence of a significant amount of inactive surface ReO_4−I species on alumina in these studies further contributed to the estimated low apparent number of active sites. The estimated fraction of surface ReO_4−II sites on alumina in prior studies is indicated in Figure 11, revealing that the surface ReO_4−II sites were the minority species and the surface ReO_4−I sites were the majority (but inactive) species for half of the studies.[1,13,30−41]

The current study, however, demonstrates that the number of active surface ReO_4−II sites for olefin metathesis is a variable number that depends on the surface ReO_4 coverage on alumina

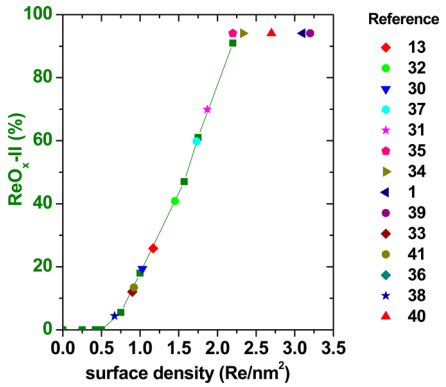

Figure 11. Comparison of estimated surface ReO_4−II concentration as a function of Re loading for supported ReO_x/Al_2O_3 catalysts that have been reported in the literature. The solid line indicates the concentration of surface ReO_4−II species as a function of Re coverage on alumina determined in the present study. The concentration of surface ReO_x-II species for other experimental data is estimated from the solid line generated in the present study. The studies reporting surface rhenia coverage higher than maximum of 2.2Re/nm^2 did not account for volatility of rhenia above this loading and, thus, can only contain a maximum of ∼2.2 Re/nm^2.

DOI: 10.1021/cs5016518
ACS Catal. 2015, 5, 1432−1444

as well as the presence of acidic surface metal oxides that block the formation of the less reactive surface ReO_4−I sites. Furthermore, "titration" with olefin is not a titration process, but actually, it is an activated chemical reaction that strongly depends on temperature. Thus, "titration" of the surface intermediates with olefins at ambient temperatures cannot react away all or even a significant fraction of the surface intermediates. The present investigation is the first direct observation that propylene selectively interacts with surface ReO_4−II sites on Al_2O_3 during propylene metathesis. With the assistance of the surface TaO_x promoter, it is even possible to design catalysts approaching 100% ReO_4−II that are all interacting with propylene. Such higher concentrations of activated sites for supported ReO_4/Al_2O_3 catalysts, as well as other supported metal oxide olefin metathesis catalysts, finally opens the opportunity to characterize the activated surface ReO_4 sites on alumina.

3.3. Molecular Structure−Reactivity Relationships of Surface ReO_4−I and ReO_4−II Sites on Al_2O_3 for Propylene Metathesis. The steady-state catalytic studies indicate that the surface ReO_4−II sites are the catalytic active sites for propylene metathesis since the surface ReO_4−I sites do not exhibit significant catalytic activity. The surface ReO_4−I sites may even be inactive and the residual minimal activity may originate from trace amounts of surface ReO_4−II sites. The propylene metathesis steady-state catalytic trend as a function of surface rhenia loading on alumina has been observed in previous kinetic studies,[1,13,42,43] but this is *the first time* that the surface dioxo ReO_4−II site on alumina has been isolated and identified as the precursor to the catalytic active site for propylene metathesis by supported ReO_4/Al_2O_3 catalysts. The major structural differences between surface ReO_4−I and ReO_4−II sites are their anchoring sites on the alumina surface and the resulting (Al−O)-Re-(O−Al) angle. The alumina anchoring sites act as potent multidentate ligands that moderate the activation of the surface ReO_4 sites for propylene metathesis. The weak interaction of surface ReO_4−I with two additional surface O atoms also certainly decreases its Lewis acidity compared to ReO_4−II.

The addition of surface TaO_x sites promotes the supported ReO_4/Al_2O_3 catalyst for propylene metathesis by occupying the surface Al_{IV} sites on the alumina support and, consequently, blocks formation of the less active surface ReO_4−I sites. As a result, the surface rhenia sites are forced to occupy the Al_V and Al_{VI} sites that result in selective formation of surface ReO_4−II sites. This is further emphasized by shifting the propylene activity curve for the supported $ReO_4/TaO_x/Al_2O_3$ catalyst by 4−5% ReO_4 toward the activity curve for Ta-free supported ReO_4/Al_2O_3 catalyst as shown in Figure 10. The overlap of the Ta-promoted and -unpromoted activity curves demonstrates that indeed the surface TaO_x sites are occupying the sites normally occupied by surface ReO_4−I and that surface TaO_x is not promoting the supported ReO_4/Al_2O_3 by chemical or electronic means, but just responsible for the formation of mostly surface ReO_4−II sites on alumina. It has been repeatedly proposed in the literature that the olefin metathesis activity is enhanced by introduction of acidic surface metal oxides (WO_x,[43] TaO_x,[44] MoO_x,[44,46] NbO_x[45,47] and VO_x[44,45]), but the current findings demonstrate that surface Brønsted acidity does not affect the intrinsic olefin metathesis reaction and the only function of acidic surface metal oxides is to block the formation of inactive ReO_4−I sites on the most reactive alumina Al_{IV} sites, which has the effect of increasing the total number of active surface ReO_4−II sites for a given Re loading.

It was estimated that the maximum amount of surface ReO_4−I species on alumina corresponds to 5% ReO_4. The lack of propylene metathesis activity for the supported 1−5% ReO_x/Al_2O_3 catalysts suggests that the maximum amount of surface ReO_4−I species corresponds to 5% ReO_4 (see Figure 10). This is also consistent with the consumption of the basic Al−OH hydroxyls (μ_1-Al_{IV}, μ_1-Al_{VI} and μ_1-Al_V at 3787, 3768, and 3743 cm^{-1}, respectively) in the IR spectrum for supported 5% ReO_4/Al_2O_3 (see Figure 7) and appearance of a ReO_4−II Raman band above 5%ReO_4 (see Figure 4).

4. CONCLUSIONS

Supported ReO_x/Al_2O_3 catalysts were found to contain two distinct isolated tetra-coordinated dioxo surface ReO_4 species on alumina (deformed ReO_4−I on basic μ_1-Al_{IV} sites and ReO_4−II on acidic μ_2-Al_{VI} and μ_3-Al_{VI} sites). DFT optimization calculations found that other surface rhenia structures were less or not stable on Al_2O_3 (tetra-coordinated mono-oxo, penta-coordinated dioxo, and tetra-coordinated trioxo). The deformed surface ReO_4−I species were not activated by propylene, but the surface ReO_4−II species were readily activated by exposure to propylene. The number of activated surface ReO_4−II species can be markedly increased by adding sacrificial surface TaO_x species that block the formation of the low activity deformed surface ReO_4−I species. These new insights allow for fundamental understanding how the (*i*) oxide support ligand controls the local surface rhenia structure and activation of the surface ReO_4 species, and (*ii*) surface metal oxide promoters increase metathesis activity by allowing for the selective formation blocking of inactive surface ReO_4−I species that increases the number of active surface ReO_4−II species. The new molecular level insights are able to resolve many confusing claims about olefin metathesis by supported ReO_4/Al_2O_3 catalysts over the years.

5. EXPERIMENTAL SECTION

5.1. Catalyst Synthesis. *5.1.1. Supported ReO_x/Al_2O_3 Catalysts.* A series of 1−18 wt % supported ReO_x/Al_2O_3 catalysts were prepared by incipient wetness impregnation of a 65−70 wt % aqueous solution of perrhenic acid, $HReO_4$ (Sigma-Aldrich), onto two different Al_2O_3 supports (Harshaw batch no. DD351, denoted as "H" and Engelhard batch no. H5433C, denoted as "E") with BET surface areas of 180 m^2/g and 170 m^2/g, respectively. Using estimations from previous studies and taking consideration of ReO_x volatility, the actual Re loadings are approximated to be 1−15.6%.[6] The supported rhenia phase did not volatilize below 6.5%, and the amount of volatilization increased nonlinearly with rhenia loading above this value. The Al_2O_3 (Harshaw) support was used for some of the studies because the low fluorescence from this alumina gave rise to higher quality in situ Raman spectra. An incipient wetness point of 1.0 mL H_2O/g was used for both supports. The alumina supports were impregnated with the aqueous perrhenic acid solution and the powders stirred for 30 min. After impregnation, the samples were initially dried overnight under ambient conditions, further dried at 120 °C for 2 h in flowing air (AirGas, ultrahigh purity (UHP)) and calcined in the flowing air by heating at 1 °C/min and held at 500 °C for 4 h (Thermodyne, furnace model 48000).

DOI: 10.1021/cs5016518
ACS Catal. 2015, 5, 1432−1444

5.1.2. Promoted Supported $ReO_x/TaO_x/Al_2O_3$ Catalysts. The supported ReO_x/Al_2O_3 catalysts were also promoted with TaO_x via incipient wetness impregnation. The supported Ta_2O_5/Al_2O_3 was prepared from a solution of tantalum ethoxide (Ta-$(OC_2H_5)_5$, Alfa Aesar, 99.999%) dissolved in toluene (Sigma-Aldrich, 99%) inside a glovebox (Vacuum Atmospheres, Omni-Lab VAC 101965) under a N_2 environment because of the air sensitivity of the Ta-ethoxide precursor. The supported Ta-ethoxide/Al_2O_3 sample was initially dried overnight in the glovebox and subsequently subjected to the same calcination procedure as applied to the supported ReO_x/Al_2O_3 catalysts. The supported Ta_2O_5/Al_2O_3 catalyst was impregnated with an aqueous $HReO_4$ solution, with the aforementioned preparation and calcination procedures, to synthesize the supported $ReO_x/Ta_2O_5/Al_2O_3$ catalysts. A reverse preparation procedure was also used to make a supported $Ta_2O_5/ReO_x/Al_2O_3$ catalyst in which the rhenia was initially impregnated and calcined prior to the addition of the tantalum oxide.

5.2. In Situ Diffuse Reflectance Ultraviolet−visible (UV−vis) Spectroscopy. The UV−vis spectra of the catalysts were collected with a Varian Cary 5E UV−vis-NIR spectrophotometer with the Harrick Praying Mantis accessory. Approximately 5−25 mg of each catalyst in finely ground powder form was loaded into an in situ environmental cell (Harrick, HVC-DR2). The catalysts were dehydrated in situ at 500 °C under oxidizing conditions (10%O_2/Ar) and spectra of the dehydrated samples were collected in the 200−800 nm range at 100 °C, using a scan rate of 15 nm/min and a signal averaging time of 0.6 s. A magnesium oxide sample was used as a standard for obtaining the background absorbance. The spectra of reference compounds, $KReO_4$ (Sigma-Aldrich, 99.98%), $NaReO_4$ (Sigma-Aldrich, 99.99%), NH_4ReO_4 (Sigma-Aldrich, >99%) and Re_2O_7 (Alfa Aesar, 99.995%) were collected under ambient conditions. The spectrum of the moisture-sensitive Re_2O_7 solid was collected with the sample in its original sealed glass vial. The Kubelka−Munk function $F(R_\infty)$ was calculated from the absorbance of the UV−vis spectra. The edge energy (E_g), or band gap, was determined by finding the intercept of the straight line for the low-energy rise of a plot of $[F(R_\infty)h\nu]^2$ versus $h\nu$, where $h\nu$ is the incident photon energy. A detailed example of this calculation can be found elsewhere.[48]

5.3. In Situ XAS (XANES/EXAFS) Spectroscopy. The in situ Re L_1-edge X-ray absorption spectroscopy (XAS) experiments were performed in transmission mode at beamlines X19A and X18B at the National Synchrotron Light Source (NSLS) at the Brookhaven National Laboratory, using ionization chamber detectors for measuring incident and transmitted beam intensities. In addition, a third ionization chamber was used to detect the beam through a reference Re foil for energy calibration and alignment purposes. A plug flow reactor cell with a quartz capillary tube (I.D./O.D. = 0.8/1.0 mm) was used for in situ dehydrated measurements. The supported ReO_x/Al_2O_3 catalysts were dehydrated at 500 °C using the same dehydration procedure mentioned above and cooled to 70 °C before the spectra were recorded. Reference compounds, trioxo(triphenylsilyloxy) rhenium(VII) (Sigma-Aldrich, 99.9%), iododioxobis (triphenylphosphine) rhenium-(V) (Sigma-Aldrich, 99.98%), trichlorooxobis (triphenylphosphine) rhenium(V) (Sigma-Aldrich, 99.99%) and rhenium(VI) oxide, ReO_3 (Alfa Aesar, 99%) were diluted with Boron Nitride (Sigma-Aldrich, 99%) to give a Re concentration of ∼5−10 wt % and measured under ambient conditions. Data processing and analysis were performed using Athena and Artemis software.

5.4. In Situ Raman spectroscopy. *5.4.1. In Situ Raman of Dehydrated Catalysts.* The Raman spectra the supported ReO_x/Al_2O_3 catalysts were obtained with a Horiba-Jobin Yvon LabRam HR instrument equipped with three laser excitations (532, 442, and 325 nm) and a liquid N_2-cooled CCD detector (Horiba-Jobin Yvon CCD-3000 V). The 442 nm laser was chosen since it minimized sample fluorescence. Spectral resolution was approximately 1 cm^{-1} and the wavenumber calibration was checked using the silica standard line at 520.7 cm^{-1}. The lasers were focused on the samples with a confocal microscope using a 50X objective (Olympus BX-30-LWD). Typically, the spectra were collected at 30 s/scan and 5 scans with a 200 μm hole.

Approximately 5−25 mg of each catalyst in powder form was loaded into an environmental cell (Harrick, HVC-DR2) with a SiO_2 window and O-ring seals which was kept cool by flowing water. The catalysts were initially dehydrated at a heating rate of 10 °C/min up to 600 °C and held for an hour under a 30 mL/min flow of 10% O_2/Ar (Airgas, certified, 9.989% O_2/Ar balance). Spectra were collected at the lowest possible temperatures as allowed by the fluorescence limitation, typically about 100 or 200 °C.

5.4.2. In Situ Raman Spectroscopy during $^{18}O-^{16}O$ Isotopic Exchange. After the aforementioned pretreatment/dehydration procedure, the $^{18}O-^{16}O$ isotope switching of the ReO_x was performed at 200 °C with $H_2{}^{18}O$ (Sigma-Aldrich, Water-^{18}O, 95 atom % ^{18}O, CAS no. 14314-42-2). The $H_2{}^{18}O$ water was manually injected into a flowing gas of 3 mL/min of 10% $^{16}O_2$/Ar and 27 mL/min of Ar (Airgas, Ar UHP 300) through a T-shaped pipe fitting with an open port using a 5 mL syringe. The minute presence of $^{16}O_2$ prevented darkening of the samples, improved the quality of the Raman spectra and was minimally involved in the oxygen isotope exchange. Plastic tubing connected the syringe to the pipe fitting and was connected throughout the experiment to prevent exposure to the ambient atmosphere. The gas lines were wrapped in heating tape and kept at ∼150 °C, at the point of injection to the cell inlet, to vaporize the $H_2{}^{18}O$ water. The injection doses were manually varied depending on the amount of exchanged ReO_x observed during the real-time monitoring with online Raman spectroscopy.

5.5. In Situ Diffuse Reflectance Infrared Fourier Transform Spectroscopy (DRIFTS). The in situ DRIFT spectra were collected with a Thermo Nicolet 8700 FT-IR spectrometer equipped with a Harrick Praying Mantis attachment (model DRA-2) for diffuse reflectance spectroscopy. Spectra were taken using a MCT detector with a resolution of 4 cm^{-1} and an accumulation of 72 scans. Approximately 5−25 mg of each catalyst in powder form was loaded into an environmental cell (Harrick, HVC-DR2). The collection of the initial background was performed by first optimizing the beam path and IR absorption signal using the height of the full Harrick sample cup, then removing the Harrick cell and placing a reflective mirror in the laser path. A spectrum was collected using the reflective mirror and was used as the background spectrum throughout the experiment. The catalysts were dehydrated at 500 °C using the same dehydration procedure mentioned above. Spectra were collected at 500, 400, 300, and 200 °C after dehydration to minimize spectral thermal

DOI: 10.1021/cs5016518
ACS Catal. 2015, 5, 1432−1444

broadening. Spectra at 200 °C are reported, unless otherwise noted.

5.6. DFT Calculations. The periodic DFT calculations have been performed in the framework of the generalized gradient approximation with the PW91 functional,[49] using the Vienna Ab Initio Simulation Package (VASP).[50−52] The one-electron wave functions are developed on a basis set of plane waves. Atomic cores are described with the projector-augmented wave method (PAW)[53] using a cutoff energy of 400 eV.

The previously validated periodic models of the γ-Al_2O_3 surface[15,16] are based on the nonspinel bulk structure.[54] The most exposed (110) plane, having an area of 74%, and the minority (100) surface, having an area of 16%, were considered for calculations.[15] The (100) and (110) surfaces have been modeled by a four- and six-layer slabs, respectively. The bottom two and three layers are frozen in the geometry of the bulk. Frequency calculations have been carried out by numerical differentiation of the force matrix. All the optimized degrees of freedom were used for the frequency calculations. The surface unit cell dimensions (Å) are a = 8.414, b = 11.180 for the (100) plane (unit formula $Al_{32}O_{48}$) and a = 8.069, b = 8.398 for the (110) plane (unit formula $Al_{24}O_{36}$). The Γ-centered 331 Monkhorst−Pack mesh provides a converged energy with respect to Brillouin-zone sampling.[55] All models consider the Re atom in the +7 oxidation state. For the graphic presentation of the structures, Materials Studio 5.5 software is used.[56]

5.7. Steady-State Propylene Metathesis Reaction. The catalytic activity measurements were performed in a fixed-bed catalytic reactor under differential conditions (propylene conversion <15%). A separate molecular sieve moisture trap was installed in the inlet propylene gas line to purify the reactants. Both inlet and outlet gas lines were heated using external electric heaters to ∼200 °C to prevent condensation of the reactants and products. The catalysts were pretreated in 10% O_2/Ar at 500 °C for 30 min before cooling down in Ar to the reaction temperature of 70 °C. Then a gas mixture of 1% propylene/1% Ar (internal standard)/He (balance) was introduced to the reactor at the flow rate of ∼100 mL/min. The products were analyzed using an online gas chromatograph (Agilent GC 6890) equipped with flame ionization (Agilent serial no.: USC250823H) and thermal conductivity (Restek product no.: PC3533) detectors. Conversion was normalized with propylene flow rate and catalyst weight to obtain reactivity, reported in mmol/g/h. The reported activity values are averages of three measurements, and the error bars indicate the upper and lower confidence levels.

■ ASSOCIATED CONTENT

Supporting Information

The following file is available free of charge on the ACS Publications website at DOI: 10.1021/cs5016518.

Supplementary information and results as noted in the text, including UV−vis spectra, DFT-optimized structures, stretching frequencies, and other relevant data (PDF)

■ AUTHOR INFORMATION

Corresponding Author

*E-mail: iew0@lehigh.edu.

Notes

The authors declare no competing financial interest.

■ ACKNOWLEDGMENTS

S.L. and I.E.W. acknowledge financial support from U.S. DOE Basic Energy Sciences (Grant No. FG02-93ER14350). Y.L. and A.I.F. acknowledge the U.S. DOE Grant No. DE- FG02-03ER15476 for supporting XAS data analysis. A.I.F. acknowledges the U.S.DOE Grant No. DE-FG02-05ER15688 for supporting the X18B beamline operations. J.H. acknowledges the computing resources from Academic Computer Centre CYFRONET AGH (Grant Nos. MNiSW/SGI3700/PK/003/2013, MNiSW/SGI4700/PK/003/2013, MNiSW/IBM_BC_HS21/PK/003/2013) and PL-Grid Infrastructure.

■ REFERENCES

(1) Mol, J. C. *Catal. Today* **1999**, *51*, 289−299.
(2) Secordel, X.; Berrier, E.; Capron, M.; Cristol, S.; Paul, J.-F.; Fournier, M.; Payen, E. *Catal. Today* **2010**, *155*, 177−183.
(3) Yoboué, A.; Susset, A.; Tougerti, A.; Gallego, D.; Ramani, S. V.; Kalyanikar, M.; Dolzhnikov, D. S.; Wubshet, S. G.; Wang, Y.; Cristol, S.; Briois, V.; La Fontaine, C.; Gauvin, R. M.; Paul, J.-F.; Berrier, E. *Chem. Commun.* **2011**, *47*, 4285−4287.
(4) Homepage for CBI Technologies. http://www.cbi.com/technologies/propylene (accessed August 28, 2014).
(5) Vuurman, M. A.; Wachs, I. E. *J. Phys. Chem.* **1992**, *96*, 5008−5016.
(6) Vuurman, M. A.; Stufkens, D. J.; Oskam, A.; Wachs, I. E. *J. Mol. Catal.* **1992**, *76*, 263−285.
(7) Kim, D. S.; Wachs, I. E. *J. Catal.* **1993**, *141*, 419−429.
(8) Mitra, B.; Gao, X.; Wachs, I. E.; Hirt, A. M.; Deo, G. *Phys. Chem. Chem. Phys.* **2001**, *3*, 1144−1152.
(9) Okal, J.; Kępiński, L.; Krajczyk, L.; Drozd, M. *J. Catal.* **1999**, *188*, 140−153.
(10) Okal, J.; Baran, J. *J. Catal.* **2001**, *203*, 466−476.
(11) Okal, J. *Appl. Catal., A* **2005**, *287*, 214−220.
(12) Bare, S. R.; Kelly, S. D.; Vila, F. D.; Boldingh, E.; Karapetrova, E.; Kas, J.; Mickelson, G. E.; Modica, F. S.; Yang, N.; Rehr, J. J. *J. Phys. Chem. C* **2011**, *115*, 5740−5755.
(13) Vicente, B. C.; Nelson, R. C.; Moses, A. W.; Chattopadhyay, S.; Scott, S. L. *J. Phys. Chem. C* **2011**, *115*, 9012−9024.
(14) Handzlik, J.; Sautet, P. *J. Catal.* **2008**, *256*, 1−14.
(15) Digne, M.; Sautet, P.; Raybaud, P.; Euzen, P.; Toulhoat, H. *J. Catal.* **2002**, *211*, 1−5.
(16) Digne, M.; Sautet, P.; Raybaud, P.; Euzen, P.; Toulhoat, H. *J. Catal.* **2004**, *226*, 54−68.
(17) Horsley, J. A.; Wachs, I. E.; Brown, J. M.; Via, G. H.; Hardcastle, F. D. *J. Phys. Chem.* **1987**, *91*, 4014−4020.
(18) Balerna, A.; Bernieri, E.; Burattini, E.; Kuz'min, A.; Lusis, A.; Purans, J.; Cikmacs, P. *Nucl. Instru. & Met. Phys. Res., Section A: Accelerators, Spectrometers, Detectors, and Associated Equipment* **1991**, *308*, 240−242.
(19) Nakamoto, K. *Infrared and Raman Spectra of Inorganic and Coordination Compounds*, 4th ed.; Wiley: New York, 1986; pp 68−75.
(20) Chen, Y.; Fierro, J. L. G.; Tanaka, T.; Wachs, I. E. *J. Phys. Chem. B* **2003**, *107*, 5243−5250.
(21) Knozinger, H.; Ratnasamy, P. *Catal. Rev. -Sci. Eng.* **1978**, *17*, 31−70.
(22) Coperet, C. *Pure Appl. Chem.* **2009**, *81*, 585−896.
(23) Wischert, R.; Copéret, C.; Delbecq, F.; Sautet, P. *ChemCatChem* **2010**, *2*, 812−815.
(24) Wischert, R.; Laurent, P.; Copéret, C.; Delbecq, F.; Sautet, P. *J. Am. Chem. Soc.* **2012**, *134*, 14430−14449.
(25) Beattie, I. R.; Gilson, T. R.; Jones, P. J. *Inorg. Chem.* **1996**, *35*, 1301−1304.
(26) Beattie, I. R.; Crocombe, R. A.; Ogden, J. S. *J. Chem. .Soc. Dalton Trans.* **1977**, 1481−1489.
(27) Beattie, I. R.; Jones, P. J. *Inorg. Chem.* **1979**, *18*, 2318−2319.
(28) Zhou, M.; Citra, A.; Liang, B.; Andrews, L. *J. Phys. Chem. A* **2000**, *104*, 3457−3465.

DOI: 10.1021/cs5016518
ACS Catal. 2015, 5, 1432−1444

(29) Bouchmella, K.; Mutin, P. H.; Stoyanova, M.; Poleunis, C.; Eloy, P.; Rodemerck, U.; Gaigneaux, E. M.; Debecker, D. P. *J. Catal.* **2013**, *301*, 233−241.
(30) Chauvin, Y.; Commereuc, D. *J. Chem. Soc., Chem. Comm.* **1992**, *6*, 462−464.
(31) Balcar, H.; Zilkova, N.; Zukal, A.; Cejka, J. *Stud. Surf. Sci. Catal.* **2008**, *174 A*, 61−66.
(32) Salameh, A.; Coperet, C.; Basset, J.; Bohm, V. P. W.; Roper, M. *Adv. Synth. Catal.* **2007**, *349*, 238−242.
(33) Kawai, T.; Kudo, H.; Suzuki, T.; Iyoda, T. *J. Mol. Catal. A: Chem.* **2000**, *158*, 533−540.
(34) McCoy, J. R.; Farona, M. F. *J. Mol. Catal.* **1991**, *66*, 51−58.
(35) Daniell, W.; Weingard, T.; Knozinger, H. *J. Mol. Catal. A: Chem.* **2003**, *204−205*, 519−526.
(36) Oikawa, T.; Ookoshi, T.; Tanaka, T.; Yamamoto, T.; Onaka, M. *Micro. Meso. Mater.* **2004**, *74*, 93−103.
(37) Schekler-Nahama, F.; Clause, O.; Commereuc, D.; Saussey, J. *Appl. Catal. A: Gen.* **1998**, *167*, 237−245.
(38) Bregeault, J.-M.; Ali, B. E.; Martin, J.; Martin, C.; Derdar, F.; Bugli, G. *J. Mol. Catal.* **1988**, *46*, 37−60.
(39) Olsthoorn, A. A.; Boelhouwer, C. *J. Catal.* **1976**, *44*, 197−206.
(40) Aldag, A. W.; Lin, C. J.; Clark, A. *J. Catal.* **1978**, *51*, 278−285.
(41) Mahmood, C. S.; Yarmo, M. A.; Hamid, S.B.D.-A. *J. Mol. Catal. A. Chem.* **2000**, *161*, 11−16.
(42) Stoyanova, M.; Rodemerck, U.; Bentrup, U.; Dingerdissen, U.; Linke, D.; Mayer, R.-W.; Lansink Rotgerink, H. G. J.; Tacke, T. *Appl. Catal. A: Gen.* **2008**, *340*, 242−249.
(43) Xiaoding, X.; Boelhouwer, C.; Vonk, D.; Benecke, J. I.; Mol, J. C. *J. Mol. Catal.* **1986**, *36*, 47−66.
(44) Ramachandran, B.; Choi, S.; Gartside, R. J.; Kleindienst, S.; Ruettinger, W.; Alerasool, S. Olefin isomerization and metathesis catalyst for manufacture of propylene. U.S. Patent 20100056839A1, March 4, 2010.
(45) Xiaoding, X.; Boelhouwer, C.; Benecke, J. I.; Vonk, D.; Mol, J. C. *J. Chem. Soc. Faraday Trans.* **1986**, *82*, 1945−1953.
(46) Flego, C.; Pollesel, P.; Ricci, M.; Romano, U. Process for preparation of 2,3-dimethylbutane. IT1324054B1, October 28, 2004.
(47) Stephan, J.; Schubert, M.; Weichert, C.; Ruppel, W.; Resch, P.; Zimdahl, S.; Mrzena, F.; Molitor, A.; Berg, S.; Fohrmann, M. Regeneration of supported rhenium oxide-doped olefin metathesis catalysts. DE10309070A1, September 16, 2004.
(48) Tian, H.; Roberts, C. A.; Wachs, I. E. *J. Phys. Chem. C* **2010**, *114*, 14110−14120.
(49) Perdew, J. P.; Chevary, J. A.; Vosko, S. H.; Jackson, K. A.; Pederson, M. R.; Singh, D. J.; Fiolhais, C. *Phys. Rev. B* **1992**, *46*, 6671−6687.
(50) Kresse, G.; Hafner, J. *Phys. Rev. B* **1993**, *47*, 558−561.
(51) Kresse, G.; Furthmüller, J. *Comput. Mater. Sci.* **1996**, *6*, 15−50.
(52) Kresse, G.; Furthmüller, J. *Phys. Rev. B* **1996**, *54*, 11169−11186.
(53) Kresse, G.; Joubert, D. *Phys. Rev. B* **1999**, *59*, 1758−1775.
(54) Krokidis, X.; Raybaud, P.; Gobichon, A.-E.; Rebours, B.; Euzen, P.; Toulhoat, H. *J. Phys. Chem. B* **2001**, *105*, 5121−5130.
(55) Monkhorst, H. J.; Pack, J. D. *Phys. Rev. B* **1976**, *13*, 5188−5192.
(56) *Materials Studio*, v. 5.5; Accelrys Software Inc.: San Diego, CA, 2010.

DOI: 10.1021/cs5016518
ACS Catal. 2015, 5, 1432−1444